PHYSICAL REVIEW A VOLUME 21, NUMBER 6 JUNE 1980

Multiple ionization and x-ray emission accompanying the cascade decay of inner-shell vacancies in Fe

V. L. Jacobs and J. Davis
Plasma Radiation Group, Code 6707, Plasma Physics Division, Naval Research Laboratory, Washington D.C. 20375

Balazs F. Rozsnyai
Lawrence Livermore Laboratory, University of California, Livermore, California 94550

John W. Cooper
Center For Absolute Physical Quantities, National Bureau of Standards, Washington D.C. 20234
(Received 18 December 1979)

A model has been developed which predicts the relative abundances of the differently charged ions and the x-ray emission spectra resulting from the cascade decay of an arbitrary distribution of inner-shell vacancies created in atoms by energetic charged particles or x rays. The multiple-ionization and x-ray production cross sections are defined in terms of the populations of the single- and multiple-vacancy states occurring in the atomic reorganization process. All allowed radiative, Auger, and Coster-Kronig transitions are taken into account in the determination of these populations. The x-ray spectra are classified in terms of characteristic lines which are due to the radiative decay of single vacancies and satellites which are associated with transitions from multiple-vacancy states. Results of calculations are presented for the creation of the initial vacancy distribution by single inner-shell electron ionization of neutral Fe with electrons and photons. Multiple ionization is found to represent only 10% of the total for electron-impact ionization but is predicted to be predominant during K- and L-shell photoionization, in agreement with experimental results obtained for the rare gases. The intensity of the $L\alpha$ satellites is always less than the $L\alpha$ characteristic line intensity for electron-impact ionization but can substantially exceed the characteristic line intensity during K-shell photoionization, in agreement with previous results obtained for medium-Z elements.

I. INTRODUCTION

High-temperature laboratory and astrophysical plasmas[1] and energetic ion-atom collisions[2] are important sources of x-ray radiation. From an analysis of the emission spectra, determinations can be made of the density and temperature of high-temperature plasmas[1,3] and the distribution of inner-shell vacancies created in atoms by energetic charged particles[4] or photons.[5] The x-ray spectra of high-temperature plasmas are usually attributed[1] to thermal electron-impact excitation of the valence-shell electrons in multiply charged ions, and the relative abundances of the various ions of a given element are usually assumed to be determined[6] by thermal electron induced ionization and recombination processes involving only the outer-shell electrons. However, it has been pointed out[7] that the ionization structure of elements in some astrophysical environments can be significantly modified by Auger transitions following inner-shell photoionization, and radiative transitions following the ionization of inner-shell electrons by suprathermal electrons can produce prominent features in the x-ray emission spectra of solar flares[8] and tokamak plasmas.[9] In this investigation we describe a general procedure for determining the relative abundances of the differently charged ions and the x-ray emission spectra resulting from the cascade decay of an arbitrary distribution of inner-shell vacancies created suddenly in atoms by energetic charged particles or x-ray photons. In the present investigation this procedure has been applied to the calculation of the x-ray production and ionization cross sections resulting from initial single shell vacancy distributions due to inner-shell electron ionization of Fe atoms by electrons and photons.

The ionization of an inner-shell electron leaves the atomic system in a very unstable electronic configuration which may decay by either a radiative transition or an Auger process. The decay of a K-shell vacancy in a heavy atom may result in new vacancies in the L and higher shells which can then be filled by further radiative or Auger transitions. This vacancy cascade process continues until all vacancies reach the outermost occupied shell, and many photons and/or Auger electrons may be emitted. Thus very high charge states are ultimately produced. The predominant abundance of very highly charged ions which has been observed[5] in the K-shell photoionization of rare-gas atoms is mainly attributable to the fact that, when inner-shell photoionization can occur, the inner-shell ionization cross sections exceed the valence-shell ionization cross sections. Al-

though there is some evidence of initial multiple ionization, which has been interpreted in the sudden approximation as electron shake off, Auger electron emission is clearly the dominant mechanism for the production of the multiple ionization observed during inner-shell photoionization. The characteristic x-ray lines which are due to radiative transitions from single inner-shell vacancy states are accompanied by satellites which are associated with radiative transitions from multiple-vacancy states. Coster-Kronig transitions, which are Auger transition involving vacancy within the same n shell, are known to provide the dominant mechanism for the production of the $L\alpha$ satellites observed[10] in the proton bombardment of medium-Z elements. Coster-Kronig transitions are also expected to play an important role in the formation of the prominent satellite structure,[11] which has been observed in heavy-ion collisions, where initial multiple ionization can be substantial.

Calculations have been reported previously for the relative abundances of the differently charged ions produced or, equivalently, for the number of Auger electrons emitted as a result of the creation of a single vacancy in each of the various nl subshells of atoms. In these calculations, either account was taken[7] only of the most important transitions for filling the various vacancy states or random selection techniques were employed.[12] Detailed models have been developed[13,14] for the L-shell characteristic line and satellite emission spectra resulting from vacancy cascades in particular medium-Z elements, but a number of specialized restrictions had to be imposed on the vacancy production and decay processes in order to reduce the complexity of the problem. Calculations have been carried out[15] for the distribution of L- and M-shell vacancies produced in the deexcitation of atoms that have been singly ionized in the K shell or in one of the L subshells, but no attempt was made to determine the populations of all possible multiple-vacancy states.

In Sec. II of this paper, we present a more comprehensive and systematic description of the atomic reorganization process in which the single-vacancy state populations and all multiple-vacancy state populations are determined by taking into account the complete set of allowed radiative and Auger transition rates. The general procedure is illustrated in Sec. III by the calculation of the multiple ionization and x-ray fluorescence probabilities associated with a single vacancy in the various nl subshells of neutral Fe. The relative abundance of the differently charged ions and the x-ray emission spectra produced by single inner-shell electron ionization of Fe atoms with electrons and photons are contrasted in Sec. IV. Our conclusions are given in Sec. V.

II. THEORY OF THE VACANCY CASCADE PROCESS

The multiple ionization and x-ray emission cross sections are most directly defined in terms of the populations of the single- and multiple-vacancy states occurring in the vacancy cascade process. In this section we present a comprehensive description of the atomic reorganization process in which the populations of the various vacancy states are systematically determined from the initial inner-shell vacancy production cross sections and all allowed elementary radiative and Auger transition rates. The calculations reported in this paper have been carried out in the LS represenation in which the j dependence of the inner-shell vacancy distribution is ignored. In the application to heavier atomic systems for which the j dependence is important, our procedure can be easily modified by redefining the vacancy states and evaluating the radiative and Auger transition rates in the j-j coupling representation.

Let α_N denote a distribution of N vacancies among the occupied nl subshells of an atomic system. For example, $1s2s^22p^6\ldots$ would represent a distribution with a single K-shell vacancy ($N=1$); $1s^22s^22p^5\ldots$ would represent a distribution that could be formed from the initial distribution by radiative decay ($N=1$), and $1s^22s2p^5\ldots$ would represent a distribution that could be formed via an Auger process ($N=2$). We shall assume that the vacancy decay processes are independent of the mechanism by which the initial distribution is formed. The total spontaneous decay rate $\Gamma(\alpha_N)$ of the distribution α_N is given by

$$\Gamma(\alpha_N)=\sum_{\beta_N} A_r(\alpha_N\rightarrow\beta_N)+\sum_{\gamma_{N+1}} A_a(\alpha_N\rightarrow\gamma_{N+1}), \quad (1)$$

where $A_r(\alpha_N\rightarrow\beta_N)$ is the rate for the radiative transition to the N-vacancy state β_N and $A_a(\alpha_N\rightarrow\gamma_{N+1})$ is the rate for the Auger transition to the $(N+1)$-vacancy state γ_{N+1}. We will take into account all radiative processes which correspond to single-electron electric-dipole transitions and all autoionization processes which correspond to two-electron radiationless transitions, where an additional vacancy is created and a single Auger electron is ejected. Åberg[16] has shown that departures from the frozen-core approximation and configuration interaction can give rise to nonvanishing transition rates for multiple emission processes, such as radiative Auger transitions and double Auger electron emissions. We have neglected these processes because they can-

not be treated within the framework of the approximations employed in the present investigation.

Let $R(\alpha_N)$ denote the rate per unit volume for the continuous production of the vacancy distribution α_N in a statistical ensemble of identical atomic systems during the initial collisional ionization or photoionization process. It is convenient to introduce an effective rate per unit volume for the production of the N-vacancy distribution α_N as

$$R_{\text{eff}}(\alpha_N) = R(\alpha_N) + \sum_{\gamma_{N-1}} M(\gamma_{N-1}) A_a(\gamma_{N-1} \to \alpha_N) . \tag{2}$$

The summation gives the contribution due to Auger transitions from the $(N-1)$-vacancy states γ_{N-1}. Rather than attempting to follow the detailed time dependence of the complete set of population densities $M(\alpha_N)$, we shall instead obtain the equilibrium solution describing the steady-state balance between the creation and decay processes for all vacancy states. Accordingly, the population densities $M(\alpha_N)$ of the states α_N corresponding to a particular value of N will be assumed to satisfy the set of simultaneous equations

$$R_{\text{eff}}(\alpha_N) + \sum_{\beta_N} M(\beta_N) A_r(\beta_N \to \alpha_N) = M(\alpha_N) \Gamma(\alpha_N) . \tag{3}$$

Equation (3), while simple in form, completely describes the atomic reorganization process. Note that a given distribution of vacancies α_N may be created in three separate ways, namely, via the initial production mechanism, via an Auger process from a distribution of N-1 vacancies γ_{N-1}, or via a radiative transition from another distribution of N vacancies β_N. We emphasize that the general formalism is not restricted to the initial formation of single vacancies, although only single-vacancy states created initially will be considered in the applications described in Secs. III and IV.

The multiple-ionization and x-ray emission cross sections are more directly defined in terms of the populations $\rho(\alpha_N)$ of the states α_N per unit current density J_i of the incident charged particles or photons. After using the definition $\rho(\alpha_N) = M(\alpha_N)/MJ_i$, where M denotes the total number of atoms per unit volume, the solution of the set of Eqs. (3) can be expressed formally by

$$\rho(\alpha_N) = \sum_{\beta_N} Q^{-1}(\alpha_N, \beta_N) \sigma_{\text{eff}}(\beta_N) . \tag{4}$$

The effective production cross section $\sigma_{\text{eff}}(\alpha_N)$ is related to the initial production cross section $\sigma(\alpha_N)$ by

$$\sigma_{\text{eff}}(\alpha_N) = \sigma(\alpha_N) + \sum_{\gamma_{N-1}} \rho(\gamma_{N-1}) A_a(\gamma_{N-1} \to \alpha_N) , \tag{2'}$$

and the transition rate matrix Q is defined by

$$Q(\alpha_N, \alpha_N) = \Gamma(\alpha_N) \tag{5}$$

and

$$Q(\alpha_N, \beta_N) = -A_r(\beta_N \to \alpha_N), \quad \alpha_N \neq \beta_N . \tag{6}$$

The inclusion of the radiative transition rates in the off-diagonal elements of the transition rate matrix Q accounts for the radiative rearrangement of the vacancy distribution α_N. In high-Z atoms radiative transitions from the K and L shells can be more probable than Auger transitions, and the populations $\rho(\alpha_N)$ cannot be obtained simply from the division of the effective production cross section $\sigma_{\text{eff}}(\alpha_N)$ by the total decay rate $\Gamma(\alpha_N)$. After the populations have been determined for all N, cross sections for the yields of various decay products can be obtained.

For a given distribution of initial vacancies, the effective populations of the single- and multiple-vacancy states following rearrangement can be obtained by a step-by-step procedure. First, we solve for the single-vacancy populations $\rho(\alpha_1)$, if any, and then we use these populations to evaluate the summation in Eq. (2'), which gives the contribution to the effective double-vacancy production cross section $\sigma_{\text{eff}}(\alpha_2)$ due to Auger transitions. Equation (4) can now be employed to obtain the double-vacancy populations $\rho(\alpha_2)$. This procedure can be continued until no further transitions can occur. The entire procedure has been efficiently programmed for a high-speed electronic computer. To the best of our knowledge the only previous attempt to obtain a systematic solution of the complete atomic reorganization problem is the Monte Carlo calculation reported by Carlson and Krause,[12] who computed the charge state distributions resulting from single inner-shell vacancies by making a random selection of the possible transitions from a table of weighted probabilities.

In order to define the multiple-ionization cross sections, it is necessary to specify the outer-shell N-vacancy states Ω_N from which further Auger transitions cannot occur. The cross section $\sigma_L(N)$ describing the loss of N electrons from the initial atomic system can be expressed in the form

$$\sigma_L(N) = \sum_{\Omega_N} \Big[\sigma(\Omega_N) + \sum_{\alpha_N} \rho(\alpha_N) A_r(\alpha_N \to \Omega_N) + \sum_{\gamma_{N-1}} \rho(\gamma_{N-1}) A_a(\gamma_{N-1} \to \Omega_N) \Big] , \tag{7}$$

where $\sigma(\Omega_N)$ are the initial outer-shell ionization cross sections, the second term gives the contribution due to radiative transitions from the N-vacancy states α_N, and the last term represents the contribution of Auger transitions from the $(N-1)$-vacancy states γ_{N-1}.

The multiple-ionization cross section defined by Eq. (7) strictly refers to an isolated atomic system. The initial stages in the cascade decay of a deep inner-shell vacancy are expected to be essentially unaffected by the presence of surrounding atomic systems or charged particles. This is a consequence of the fact that Auger transitions usually occur between neighboring shells, as has been pointed out by Carlson, Hunt, and Krause.[5] However, the final stages, in which a large number of vacancies are transferred to the outer shells, can be significantly affected by electron capture processes. In a companion paper[17] it will be shown that the static screening effect produced by a high-density plasma can cause an energetic opening of the channel for certain Coster-Kronig transitions. This can have a significant effect on the distributions of the higher-charge states.

The cross section describing the emission of x-ray radiation in the transition $\alpha_N \to \beta_N$ can be simply defined in terms of the populations $\rho(\alpha_N)$ by

$$\sigma_r(\alpha_N \to \beta_N) = \rho(\alpha_N) A_r(\alpha_N \to \beta_N) . \tag{8}$$

If the radiative rearrangement of the N-vacancy distribution α_N is neglected in Eq. (4), then Eq. (8) reduces to the familiar product of the effective production cross section $\sigma_{\text{eff}}(\alpha_N)$ and the fluorescence yield $A_r(\alpha_N \to \beta_N)/\Gamma(\alpha_N)$. Radiative decays of multiple-vacancy $(N>1)$ states generate satellites which usually lie on the short-wavelength side of the characteristic x-ray lines, which are associated with the radiative decay of single-vacancy $(N=1)$ states. Krause, Wuilleumier, and Nester[13] have pointed out that the spectral feature which is conventionally identified as the true characteristic x-ray line may contain a large percentage of unresolvable satellites. More recent studies have focused on the broadening of the characteristic x-ray lines which is attributable to satellite transitions.[18,19] Knudson *et al.*[11] have observed that the satellite structure produced in heavy-ion atom collisions is much more intense than can be generated by ionization with electrons or protons. After the complete set of populations $\rho(\alpha_N)$ for all α_N have been obtained, Eq. (8) can be employed to evaluate the intensity of the satellite radiation produced by the decay of all multiple-vacancy distributions α_N with $N>1$, which can be created by both initial multiple-ionization and Auger processes.

III. MULTIPLE IONIZATION AND x-RAY FLUORESCENCE PROBABILITIES ASSOCIATED WITH THE INDIVIDUAL *nl* SUBSHELLS

The general procedure described in Sec. II will be illustrated in this section by calculating the multiple-ionization and x-ray fluorescence probabilities resulting from the cascade decay of a single vacancy in the various inner shells of neutral Fe atoms. In addition to providing a better understanding of the basic mechanisms leading to multiple-ionization and x-ray emission in atomic inner-shell ionization processes, the charge state and x-ray emission probabilities associated with the individual nl subshells can be combined with the appropriate single-vacancy production cross sections to obtain the cross sections for multiple-ionization and x-ray emission. It should be emphasized that this analysis is based on the assumptions that initial multiple ionization can be neglected and that the vacancy creation and decay processes can be treated independently.

We have simplified our calculations by adopting a model of the neutral Fe atom in which the valence-shell configuration is $3d^8$ instead of $3d^6 4s^2$.

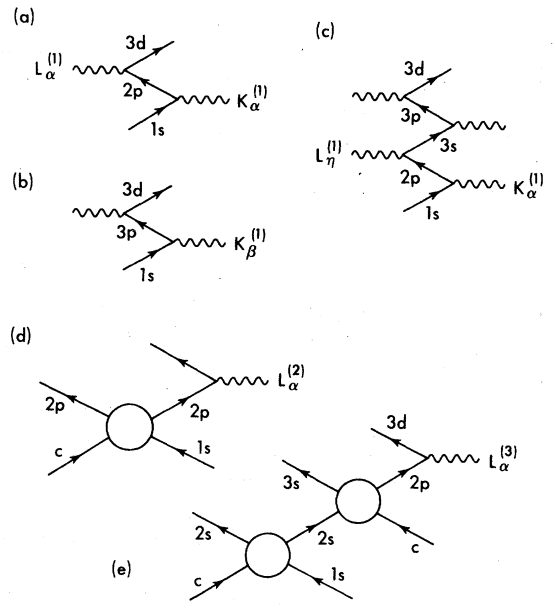

FIG. 1. Feynman-type diagrams representing the radiative rearrangement of the single-vacancy distribution and the generation of the characteristic line and some of the satellite radiation during the cascade decay of a single K-shell vacancy in neutral Fe. Straight lines represent single nl vacancy states, and continuum electron vacancy states are denoted by c. Photon emission is represented by a wavy line, while Auger processes are representated by circles. Superscripts, e.g., $L^{(1)}$ refer to the numbers of vacancies.

This approximation is not expected to have a significant effect on our results. The effects of a single vacancy in the nl subshell can be determined by replacing the initial production cross sections in Eq. (2′) by $\delta(N,1)\delta(\alpha_N,nl)$. Equations (7) and (8) will then define dimensionless quantities which can be interpreted as the probabilities for multiple-ionization and x-ray fluorescence resulting from the cascade decay process. The radiative rearrangement of the single-vacancy distribution and the generation of the characteristic line and some of the satellite radiation during the cascade decay of a single K-shell vacancy in Fe can be represented by the Feynman-type diagrams in Fig. 1. The $1s \rightarrow 2p$ $K\alpha$ radiative transition which can fill the initial K-shell vacancy is also a mechanism for the excitation of the $2p \rightarrow 3d$ $L\alpha$ characteristic line, as shown in Fig. 1(a). Figures 1(b) and 1(c) indicate how other characteristic lines may be produced by the transfer of single vacancies due to radiative processes. Satellites associated with the characteristic line radiations are the result of radiative transitions which occur after one or more Auger processes. This is indicated in Fig. 1(d), which shows a diagram for the formation of a double $2p$ vacancy followed by $L\alpha$ radiation, and Figure 1(e), which represents the formation of $2s$, $2p$, and $3s$ vacancies by Auger processes before $L\alpha$ radiation is emitted. The Auger processes are represented in Fig. 1 by contracted diagrams, which indicate that both the direct and exchange contributions are taken into account.

The first-order nonrelativistic perturbation theory expressions for the radiative and Auger transition rates in neutral Fe have been evaluated in the frozen-core approximation by using Hartree-Slater wave functions. A detailed description of the evaluation of these transition rates will be presented in a companion paper.[17] The creation of multiple vacancies causes photon energy shifts and may result in an energetic closing of the channel for certain Coster-Kronig transitions.[10] In the determination of the populations of the multiple-vacancy states, no attempt was made to correct the radiative or Auger transition rates for these effects. Allowance for these corrections to the transition energies as well as for other departures from the frozen-core approximation would require an immensely more complex calculation. However, it is straightforward to systematically correct the various transition rates in order to take into account the number of remaining electrons in the relevant nl subshells. These modifications were accomplished by employing the relationships[6,20]

$$A_a(n_1l_1^{N_1},n_3l_3^{N_3},n_4l_4^{N_4}\rightarrow n_1l_1^{N_1-1},n_3l_3^{N_3+1},n_4l_4^{N_4+1}) = N_1\frac{(4l_3+2-N_3)}{(4l_3+2)}\frac{(4l_4+2-N_4)}{(4l_4+2)}A_a(n_1l_1\rightarrow n_3l_3,n_4l_4)\,, \quad (9)$$

$$A_a(n_1l_1^{N_1},n_3l_3^{N_3}\rightarrow n_1l_1^{N_1-1},n_3l_3^{N_3+2}) = \frac{N_1}{2}\frac{(4l_3+2-N_3)}{(4l_3+2)}\frac{(4l_3+1-N_3)}{(4l_3+1)} \times A_a(n_1l_1\rightarrow n_3l_3^2)\,, \quad (10)$$

and

$$A_r(n_1l_1^{N_1},n_2l_2^{N_2}\rightarrow n_1l_1^{N_1-1},n_2l_2^{N_2+1}) = N_1\frac{(4l_2+2-N_2)}{(4l_2+2)}A_r(n_1l_1\rightarrow n_2l_2)\,, \quad (11)$$

where the number of vacancies in the n_il_i subshell is denoted by N_i.

The substitution of $\delta(N,1)\delta(\alpha_N,nl)$ for the initial vacancy production cross sections in Eq. (2′) converts the x-ray emission cross section defined by Eq. (8) into the probability $P^{(N)}(nl,n_1l_1\rightarrow n_2l_2)$ that a single vacancy in the nl subshell will result in photon emission through the transition $n_1l_1\rightarrow n_2l_2$ in a state consisting of N vacancies. The complete set of fluorescence probabilities $P^{(N)}(nl,n_1l_1\rightarrow n_2l_2)$ clearly provides a more detailed description of the emission of radiation than the usual fluorescence yields $P^{(1)}(nl,nl\rightarrow n_2l_2)$, which describe only the characteristic line emission ($N=1$) from the initial vacancy state ($n_1l_1=nl$). In Table I we present for each initial nl vacancy our results for the fluorescence probabilities associated with the various characteristic lines. We also give the total satellite radiation probability associated with each characteristic line. No attempt has been made to distinguish between observable and nonobservable satellites since this distinction depends on spectral resolution. In addition, we have not subdivided the satellite distributions into the separate contributions from double, triple, and higher states of ionization although these are distinguishable in our calculation.

The fluorescence probability $P^{(1)}(1s,1s\rightarrow 2p)$ is found to be in good agreement with the K-shell fluorescence yield given by Bambynek *et al.*,[21] and the L-shell fluorescence yields are in qualitative agreement. The emission of satellite radiation following one or more Auger processes is found to be more probable than the excitation of the corresponding characteristic line by the radiative

TABLE I. X-ray fluorescence probabilities $P^{(N)}$ $(nl,\ n_1l_1 \rightarrow n_2l_2)$ resulting from the cascade decay of single inner-shell vacancies in Fe.

Radiative transition $n_1l_1 \rightarrow n_2l_2$	Initial vacancy state nl 1s	2s	2p	3s	3p
	Characteristic line radiation ($N=1$)				
$1s \rightarrow 2p$	0.27				
$1s \rightarrow 3p$	0.33(−1) [a]				
$2s \rightarrow 2p$		0.59(−5)			
$2s \rightarrow 3p$		0.28(−3)			
$2p \rightarrow 3s$	0.60(−4)	0.13(−8)	0.22(−3)		
$2p \rightarrow 3d$	0.83(−3)	0.18(−7)	0.30(−2)		
$3s \rightarrow 3p$	0.43(−9)	0.92(−14)	0.16(−8)	0.71(−5)	
$3p \rightarrow 3d$	0.53(−6)	0.44(−8)	0.25(−13)	0.11(−9)	0.16(−4)
	Satellite line radiation ($N>1$)				
$2s \rightarrow 2p$	0.16(−5)				
$2s \rightarrow 3p$	0.83(−4)				
$2p \rightarrow 3s$	0.32(−3)	0.25(−3)			
$2p \rightarrow 3d$	0.33(−2)	0.28(−2)			
$3s \rightarrow 3p$	0.30(−5)	0.46(−5)	0.85(−6)		
$3p \rightarrow 3d$	0.45(−4)	0.50(−4)	0.21(−4)	0.17(−4)	

[a] Numbers in parentheses are powers of ten.

filling of the initial vacancy. For an initial $L_{\rm I}$-subshell vacancy, the most probable photoemission process is found to be the $2p \rightarrow 3d$ $L\alpha$ satellite emission following a $L_{\rm I} - L_{\rm II,III}$ M Coster-Kronig transition.

The replacement of the initial vacancy production cross sections in Eq. (2′) by $\delta(N,1)\delta(\alpha_N, nl)$ changes Eq. (7) into the definition of the probability $P(nl, N_a)$ that a single nl vacancy will result in the ejection of N_a Auger electrons. These probabilities can also be interpreted as the relative abundances of the various final ionic products with charges $Z = N_a + 1$. The single- and multiple-ionization probabilities resulting from the cascade decay of single inner-shell vacancies in neutral Fe are displayed in Fig. 2 by vertical bars located above each value of the final charge. Analogous results for the rare gases have been reported in the form of histograms by Carlson, Hunt, and Krause,[5] who employed various approximations for the subshell photoionization cross sections in order to deduce from their x-ray absorption data the charge state distributions associated with each initial nl vacancy.

Figure 2 also shows for each initial nl vacancy the mean charge $\langle Z \rangle$ obtained from the evaluation of the relationship

$$\langle Z \rangle = \sum_Z Z\delta(Z, N_a + 1)P(nl, N_a). \qquad (12)$$

Equation (12) is appropriate because of the fact that the ionization probabilities $P(nl, N_a)$ corresponding to each nl value are normalized to unity. As anticipated, the mean charge is found to increase with increasing binding energy of the subshell in which the initial vacancy is created. The only exception to this trend occurs in the case of a K-shell vacancy, which gives rise to a lower mean charge than an $L_{\rm I}$-subshell vacancy. This exception is attributable to radiative transitions which transfer the initial K-shell vacancy to the $L_{\rm II,III}$ and $M_{\rm II,III}$ subshells without ionization and to the fact that Auger processes are more probable

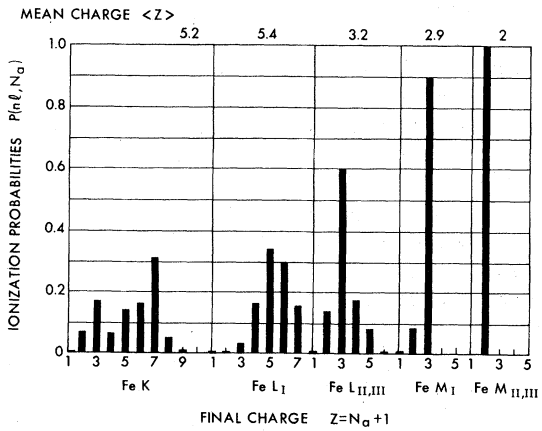

FIG. 2. Single- and multiple-ionization probabilities and the mean charge resulting from the cascade decay of a single vacancy in the various nl subshells of neutral Fe atoms. The emission of N_a Auger electrons leads to a final charge of $Z = N_a + 1$.

for the $L_{\rm I}$-subshell than for the K shell. Note also that for $3p\,(M_{\rm II,III})$ vacancy formation the ion is left in a doubly charged state with almost unit probability due to the large probability of $3p \rightarrow 3d^2$ Coster-Kronig transitions.

IV. SINGLE INNER-SHELL ELECTRON IONIZATION BY ELECTRONS AND PHOTONS

In order to evaluate the multiple-ionization and x-ray emission cross sections, it is necessary to employ realistic approximations for the single-vacancy production cross sections. The subshell cross sections for electron-impact ionization of neutral Fe were obtained by using the formula[22]

$$\sigma_e(nl) = \pi a_0^2 \left(\frac{I_H}{I_{nl}}\right)^2 \left(\frac{N_{nl}}{u}\right) \left\{ A(nl) \ln(u) + D(nl)\left(1-\frac{1}{u}\right)^2 + \left[\frac{C(nl)}{u} + \frac{d(nl)}{u^2}\right]\left(1-\frac{1}{u}\right)\right\}, \tag{13}$$

where E is the incident electron energy, I_{nl} is the ionization energy of the nl subshell which contains N_{nl} electrons, and $u = E/I_{nl}$. The remaining symbols have their conventional meaning. The coefficients $A(nl)$, $D(nl)$, $C(nl)$, and $d(nl)$ were obtained by Moors, Golden, and Sampson,[22] who fitted the results of their Coulomb-Born-exchange calculations for hydrogenic ions to this formula. An important feature of electron-impact ionization is that the valence-shell ionization cross section always exceed the inner-shell ionization cross sections, even at relatively high energies.[23] The simple representation of electron-impact ionization given by Eq. (13) has this feature.

The photoionization cross sections for the various nl subshells of neutral Fe have been calculated using a Hartree-Slater central-potential model by Reilman and Manson,[24] and their results were employed for incident photon energies up to 100 Ry. For higher energies, the relativistic cross sections obtained by Scofield[25] were adopted. The two different calculations are in very good agreement in the energy region below the K-shell threshold. The relative importance of the individual nl-subshell cross sections at a given incident photon energy E can be anticipated from the properties of the hydrogenic expression given by[1]

$$\sigma_P(nl) = \frac{64\pi\alpha a_0^2}{3^{3/2}} \frac{N_{nl}}{2l+1} \left(\frac{I_H}{E}\right)^3 \frac{Z^4}{n^3} g(nl). \tag{14}$$

The Gaunt factor $g(nl)$ is close to unity at the ionization threshold and decreases asymptotically as $E^{-0.5-l}$. It can be seen that photoionization from the most tightly bound nl subshell that can be ionized will be more probable than photoionization from the higher-n shells, and that for a given n the lowest value of l will have the largest asymptotic cross section. This behavior of the subshell photoionization cross sections is indeed exhibited

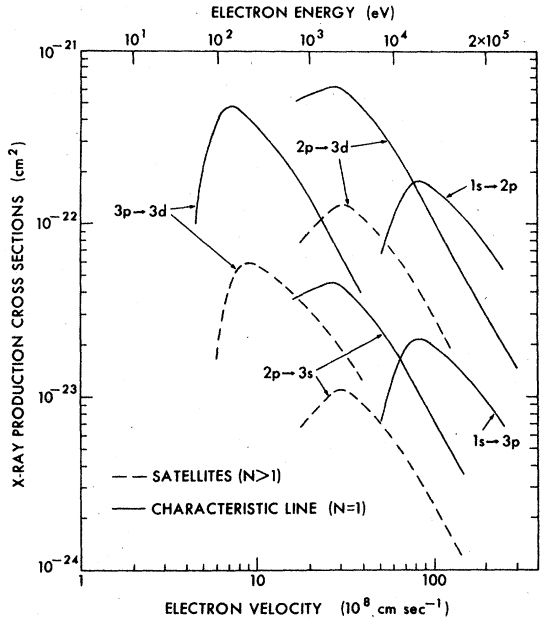

FIG. 3. X-ray production cross sections resulting from the single inner-shell electron ionization of neutral Fe by incident electrons. Results are given only for the most intense transitions.

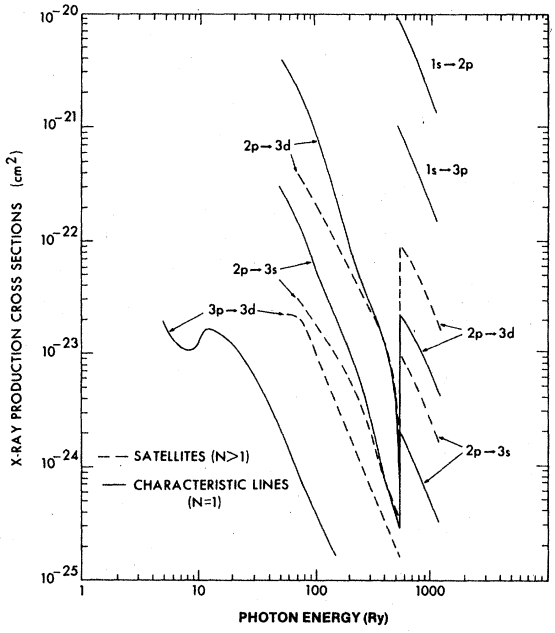

FIG. 4. X-ray production cross sections resulting from the single inner-shell electron photoionization of neutral Fe. Results are given only for the most intense transitions.

by the nonhydrogenic results and is in marked contrast with the variation of the electron-impact ionization cross sections.

The cross section $\sigma_r^{(N)}(n_1l_1 \rightarrow n_2l_2)$ describing the emission of x-ray radiation in the transition $n_1l_1 \rightarrow n_2l_2$ from an N-vacancy state is obtained from the individual inner-shell vacancy creation cross sections $\sigma(nl)$ and the fluorescence probabilities $P^{(N)}(nl, n_1l_1 \rightarrow n_2l_2)$ by means of the expression

$$\sigma_r^{(N)}(n_1l_1 \rightarrow n_2l_2) = \sum_{nl} P^{(N)}(nl, n_1l_1 \rightarrow n_2l_2)\sigma(nl) . \quad (15)$$

The cross sections for the production of the most intense emissions by electron-impact ionization are presented in Fig. 3, while the corresponding results for photoionization are displayed in Fig. 4. Each broken curve gives the total satellite contribution ($N>1$) associated with the characteristic line ($N=1$). No $1s \rightarrow np$ satellite radiation is predicted by the present calculations because of the neglect of initial double K-shell ionization. As anticipated, the $2p \rightarrow 3d$ $L\alpha$ characteristic line emission is found to be the most intense in each case, except at high energies where the K-shell lines become dominant.

TABLE II. Intensity of the $2p \rightarrow 3d$ $L\alpha$ satellite radiation, relative to the intensity of the $L\alpha$ characteristic line radiation, resulting from the single inner-shell electron ionization of neutral Fe atoms by electrons and photons. Both the hidden and observable satellites are taken into account.

Incident electron energy (keV)	Relative intensity
1.13	0.16
4.55	0.23
1.00(1)[a]	0.25
1.80(1)	0.26
2.84(1)	0.27
7.90(1)	0.29
1.75(2)	0.30
Incident photon energy (keV)	**Relative intensity**
9.52(−1)	0.17
1.08	0.18
1.22	0.20
1.36	0.27
1.50	0.27
2.00	0.34
3.00	0.53
4.00	0.76
5.00	1.00
6.00	1.00
7.00	1.26
7.13	3.60
8.00	3.63
1.00(1)	3.77
1.50(1)	3.81

[a]Numbers in parentheses are powers of ten.

The ratio of the satellite intensity to the characteristic line intensity is significantly affected by the pronounced differences in the incident energy behavior of the subshell cross sections for electron-impact ionization and photoionization. The relative intensity of the $L\alpha$ satellite radiation is tabulated as a function of the incident energy for both cases in Table II. Below the K-shell ionization threshold the $L\alpha$ satellite emission can be produced only by $L_I \rightarrow L_{II,III}$ M Coster-Kronig transitions, and the relative $L\alpha$ satellite intensity is proportional to the partial cross section ratio $\sigma(2s)/\sigma(2p)$, which attains its maximum value in the photoionization process. The additional Auger transitions, such as those represented in Fig. 1, which can occur above the K-shell ionization threshold result in an order-of-magnitude increase in the relative $L\alpha$ satellite intensity in the case of photoionization. The maximum value of 3.8 is in excellent agreement with the maximum relative $L\alpha$ satellite intensity which has been predicted for Zr.[13] The maximum ratio of 0.30 found for electron-impact ionization is in good qualitative agreement with the experimental results obtained from the bombardment of medium-Z elements by 2.5-MeV protons,[10] which corresponds approximately to an incident electron energy of 1.3 keV.

The cross section $\sigma_L(N_a+1)$ describing the loss

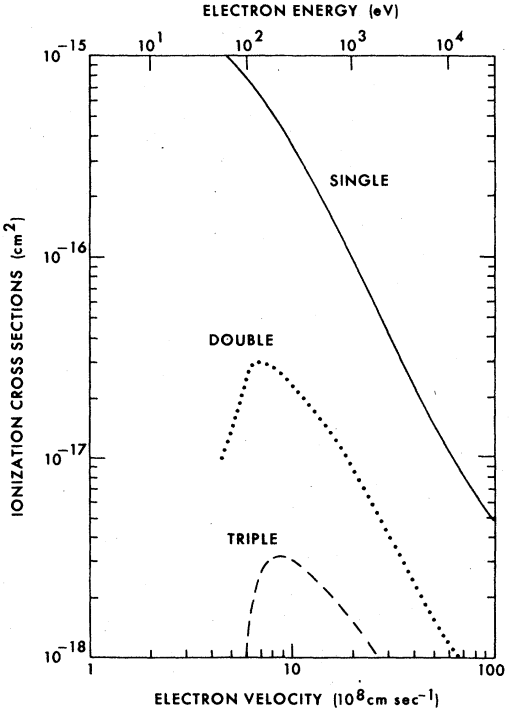

FIG. 5. Single- and representative multiple-ionization cross sections resulting from the single inner-shell electron ionization of neutral Fe by incident electrons.

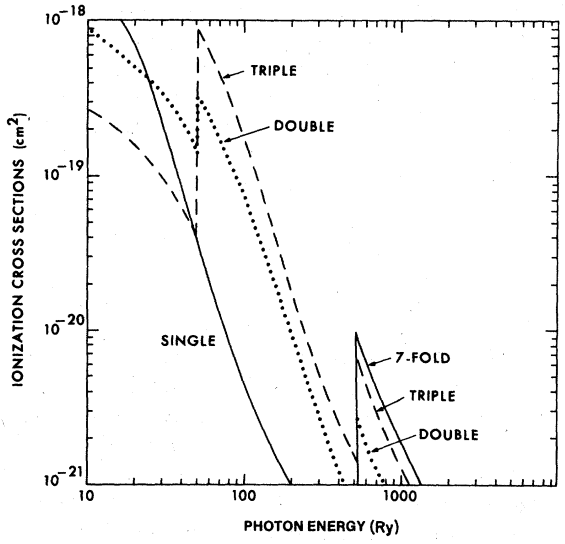

FIG. 6. Single- and representative multiple-ionization cross sections resulting from the single inner-shell electron photoionization of neutral Fe.

of N_a+1 electrons from the initial atomic system can be obtained from the expression

$$\sigma_L(N_a+1) = \sum_{nl} P(nl, N_a)\sigma(nl)\,, \tag{16}$$

where $P(nl, N_a)$ are the probabilities for the ejection of N_a Auger electrons following the creation of a single vacancy in the various nl subshells. A representative selection of the results for incident electrons and photons is displayed in Figs. 5 and 6, respectively. The complete set of single-and multiple-ionization cross sections resulting from inner-shell photoionization is presented over an extensive incident photon energy range in Table III. In marked contrast to electron-impact ionization, where multiple ionization represents no more than 10% of the total, multiple ionization can be seen to be predominant during K- and L-shell photoionization. This phenomenon is directly attributable to the fact that the most tightly bound nl electron that can be ionized will have a larger cross section for photoionization than the electrons in the higher-n shells.

It is well known[10] that multiple ionization can result in an energetic closing of the channels for the strong Coster-Kronig and/or super Coster-Kronig transitions which play the dominant role in the decay of $L_{\rm I}$, $M_{\rm I}$, and $M_{\rm II,III}$ vacancy states. The inclusion of this effect, which has not been attempted in the present calculation, would result in smaller yields for the higher charge states but would enhance the fluorescence yields. In addition the effects of multiplet structure, which are not included in our calculation, have been found to be important in the evaluation of Auger transition rates and fluorescence yields of highly charged atoms.[26] Consequently, our results for the fluorescence yields and satellite intensities should not be applied to the interpretation of experiments in which multiplet structure is resolved.

TABLE III. Single- and multiple-ionization cross sections $\sigma_L(N_I)$ (in cm^2) resulting from the single inner-shell electron photoionization of neutral Fe atoms. N_I is the total number of ejected electrons, including N_I-1 Auger electrons.

Photon energy (Ry)	$N_I=1$	$N_I=2$	$N_I=3$	$N_I=4$	$N_I=5$	$N_I=6$	$N_I=7$
30	0.21(–18) [a]	0.36(–18)	0.91(–19)				
40	0.93(–19)	0.23(–18)	0.57(–19)				
50	0.45(–19)	0.13(–18)	0.40(–19)				
60	0.28(–19)	0.23(–18)	0.63(–18)	0.17(–18)	0.83(–19)	0.28(–20)	
70	0.16(–19)	0.16(–18)	0.45(–18)	0.14(–18)	0.10(–18)	0.41(–19)	0.20(–19)
80	0.11(–19)	0.12(–18)	0.32(–18)	0.10(–18)	0.76(–19)	0.32(–19)	0.16(–19)
90	0.65(–20)	0.91(–19)	0.26(–18)	0.84(–19)	0.62(–19)	0.27(–19)	0.13(–19)
100	0.49(–20)	0.71(–19)	0.19(–18)	0.64(–19)	0.49(–19)	0.22(–19)	0.11(–19)
110	0.36(–20)	0.52(–19)	0.14(–18)	0.47(–19)	0.38(–19)	0.19(–19)	0.95(–20)
147	0.13(–20)	0.24(–19)	0.65(–19)	0.23(–19)	0.20(–19)	0.11(–19)	0.56(–20)
220	0.30(–21)	0.74(–20)	0.19(–19)	0.75(–20)	0.78(–20)	0.49(–20)	0.25(–20)
293	0.10(–21)	0.30(–20)	0.81(–20)	0.34(–20)	0.39(–20)	0.27(–20)	0.14(–20)
367	0.43(–22)	0.16(–20)	0.43(–20)	0.19(–20)	0.23(–20)	0.16(–20)	0.83(–21)
440	0.22(–22)	0.90(–21)	0.25(–20)	0.11(–20)	0.15(–20)	0.11(–20)	0.55(–21)
520	0.11(–22)	0.52(–21)	0.15(–20)	0.71(–21)	0.97(–21)	0.73(–21)	0.37(–21)
524	0.37(–22)	0.28(–20)	0.69(–20)	0.30(–20)	0.57(–20)	0.61(–20)	0.11(–19)
588	0.28(–22)	0.21(–20)	0.52(–20)	0.23(–20)	0.43(–20)	0.46(–20)	0.81(–20)
734	0.15(–22)	0.12(–20)	0.28(–20)	0.13(–20)	0.24(–20)	0.26(–20)	0.45(–20)
1100	0.44(–23)	0.37(–21)	0.91(–21)	0.41(–21)	0.79(–21)	0.86(–21)	0.15(–20)

[a] Numbers in parentheses are powers of ten.

V. CONCLUSIONS

We have developed a systematic procedure for determining the relative abundances of the differently charged ions and the characteristic x-ray line and satellite emission spectra resulting from the cascade decay of an arbitrary distribution of inner-shell vacancies created in atoms by energetic charged particles and x-ray photons. Single ionization and characteristic x-ray line emission are found to be predominant when single inner-shell electron ionization is induced in neutral Fe by incident electrons. In contrast, K-shell photoionization results predominantly in multiple ionization and leads to an $L\alpha$ satellite intensity which substantially exceeds the corresponding characteristic line intensity. In future investigations, we hope to allow for some degree of initial multiple ionization and to treat heavy-ion collisions where substantial satellite emission has been observed.

ACKNOWLEDGMENTS

The authors wish to thank S. T. Manson for providing unpublished results for the partial photoionization cross sections. This work was supported by the Office of Naval Research.

[1]H. R. Griem, *Plasma Spectroscopy* (McGraw-Hill, New York, 1964).
[2]J. D. Garcia, R. J. Fortner, and T. M. Kavanagh, Rev. Mod. Phys. 45, 111 (1973).
[3]A. H. Gabriel and C. Jordan, in *Case Studies in Atomic Collision Physics* II, edited by E. W. McDaniel and M. R. C. McDowell (North-Holland, New York, 1972).
[4]P. Richard, in *Atomic Inner-Shell Processes*, Vol. I, edited by B. Crasemann (Academic, New York, 1975).
[5]T. A. Carlson, W. E. Hunt, and M. O. Krause, Phys. Rev. 151, 41 (1966).
[6]V. L. Jacobs, J. Davis, P. C. Kepple, and M. Blaha, Ap. J. 211, 605 (1977).
[7]J. C. Weisheit, Ap. J. 190, 735 (1974).
[8]U. Feldman, S. Goldsmith, J. L. Schwob, and G. Doschek, Ap. J. 201, 225 (1975).
[9]M. Bitter, K. W. Hill, N. R. Sauthoff, P. C. Efthimion, E. Meservey, W. Roney, S. Von Goeler, R. Horton, M. Goldman, and W. Stodiek, Phys. Rev. Lett. 43, 129 (1979).
[10]B. L. Doyle and S. M. Shafroth, Phys. Rev. A 19, 1433 (1979).
[11]A. R. Knudson, D. J. Nagel, P. G. Burkhalter, and K. L. Dunning, Phys. Rev. Lett. 26, (1971).
[12]T. A. Carlson and M. O. Krause, Phys. Rev. 137, A1655 (1965).
[13]M. O. Krause, F. Wuilleumier, and C. W. Nester, Phys. Rev. A 6, 871 (1973).
[14]J. W. Cooper (unpublished).
[15]P. V. Rao, M. H. Chen, and B. Crasemann, Phys. Rev. A 5, 997 (1972).
[16]T. Åberg, in *Atomic Inner-Shell Processes*, Vol. I, edited by B. Crasemann (Academic, New York, 1975).
[17]B. F. Rozsnyai, V. L. Jacobs, and J. Davis, Phys. Rev. A 21, 1798 (1980).
[18]P. Chevallier, M. Travennier, and J. P. Briand, J. Phys. B 11, L171 (1978).
[19]R. E. Lavilla, Phys. Rev. A 19, 717 (1979).
[20]E. J. McGuire, in *Atomic Inner-Shell Processes*, edited by B. Crasemann (Academic, New York, 1975), Vol. I.
[21]W. Bambynek, B. Crasemann, R. W. Fink, F. U. Freund, H. Mark, C. P. Swift, R. E. Price, and P. V. Rao, Rev. Mod. Phys. 44, 716 (1972).
[22]D. L. Moores, L. B. Golden, and D. H. Sampson, J. Phys. B 13, 385 (1980).
[23]D. H. Madison and E. Merzbacker, in *Atomic Inner-Shell Processes*, Vol. I, edited by B. Crasemann (Academic, New York, 1975).
[24]R. F. Reilman and S. T. Manson, Phys. Rev. A 18, 2124 (1978).
[25]J. H. Scofield, Lawrence Livermore Laboratory, Report No. UCRL-51326, 1973 (unpublished).
[26]M. H. Chen and B. Crasemann, Phys. Rev. A 12, 959 (1975).